Available online at www.sciencedirect.com

SciVerse ScienceDirect

Ceramics International 38 (2012) 6455–6460

CERAMICS INTERNATIONAL

www.elsevier.com/locate/ceramint

Temperature dependent conductivity and structural properties of sol–gel prepared holmium doped Bi_2O_3 nanoceramic powder

İ. Taşçıoğlu[a], M. Arı[b], İ. Uslu[c], S. Koçyiğit[c,*], Y. Dağdemir[b], V. Çorumlu[b], Ş. Altındal[a]

[a]*Physics Department, Faculty of Arts and Sciences, Gazi University, Ankara, Turkey*
[b]*Physics Department, Faculty of Sciences, Erciyes University, Kayseri, Turkey*
[c]*Department of Chemistry Education, Gazi University, Ankara, Turkey*

Received 1 March 2012; received in revised form 7 May 2012; accepted 8 May 2012
Available online 15 May 2012

Abstract

Holmium (Ho)-doped Bi_2O_3 nanoceramic powders derived from sol–gel method have been studied in terms of structural, morphological, and electrical properties. The morphology of the nanoceramic materials was analyzed by scanning electron microscopy (SEM) and their structure by X-ray powder diffraction (XRD). Temperature dependence of DC conductivity measurements of nanoceramic powders were carried out by using DC four-point probe technique (4PPT) in air at temperatures ranging from 702 to 1169 K. Electrical conductivity results demonstrate that there is a sharp increase at around 973 K, which indicates an existence of order–disorder transition. This result supported by the Differential Thermal Analyzer (DTA) curve and XRD pattern which show that the sample has stable high oxygen ionic conductivity fluorite type face centered cubic δ-phase. Electrical characteristics also show that the DC conductivity in the studied materials obeys Arrhenius relation with different activation energies and conduction mechanisms: two temperature regions with activation energies $E_{a1}=1.40$ eV (702–993 K) and $E_{a2}=0.66$ eV (1006–1169 K). The analysis of experimental data revealed that the translation motion of the charge carrier, oxygen vacancies, and space charge polarization are responsible for the change in activation energy as a function of temperature.

Keywords: A. Sol–gel processes; B. Nanocomposites; C. Electrical properties; C. Thermal properties

1. Introduction

δ-Phase Bi_2O_3 is an oxide ionic conductor, which is a solid oxide with high oxygen ionic conductivity. Because of its novel properties and wide potential applications such as fuel cells, high-temperature oxygen pumps and many sensors, it is recognized as one of the most important oxide ionic conductors [1–6].

The δ-phase is one of the six known poly-types of Bi_2O_3 solid [7] (α, β, γ, δ, ε, and ω) and it is stable only in the temperature range from 1003 K to its melting temperature of 1098 K [2]. However, by the addition of appropriate dopants, which include rare-earth elements (Ho^{3+}, Y^{3+}, Er^{3+}, Gd^{3+}) and many oxide impurities [8,9], δ-Bi_2O_3 based ceramic materials can be stabilized even at low temperatures. Rare earth elements are known to exhibit useful functions of stabilizing the temperature dependence of relative dielectric constant besides lowering the dissipation factor in dielectric ceramics [10]. Ho^{3+}, which is used in this study, is one of the preferred rare earth dopants, since, depending on composition and processing conditions, room temperature resistivity as low as 3 Ω cm can be obtained [11]. Consequently, various experimental surveys have been published by incorporating rare-earth dopants into δ-Bi_2O_3 [1–3,8].

Most of the Bi-based δ-phase electrolyte materials show two distinct temperature dependence conductivity characters. This kind of behavior called the order–disorder transition which occurs at high temperature region could be attributed to a charge transfer between the oxygen ions and vacant orbital of cations in the distorted crystal structure. In other

*Corresponding author. Tel.: +90 312 202 8017; fax: +90 312 202 8041.
E-mail address: sergas_29@hotmail.com (S. Koçyiğit).

0272-8842/$36.00
http://dx.doi.org/10.1016/j.ceramint.2012.05.022

words, oxygen vacancies are partly responsible for the order–disorder transition [10,12].

In this work, holmium doped Bi_2O_3 nanocrystalline ceramic powder was synthesized, using poly(vinyl alcohol) (PVA) as polymer precursor, in order to investigate crystal structure and examine electrical properties of polymer derived holmium doped Bi_2O_3 using sol–gel technique. This technique was used due to its advantages such as the applicability of polymer derived ceramics in polymer processing techniques, the homogeneity of the precursors on a molecular level, the low processing temperatures when compared to conventional powder sintering methods [13–17].

The present work is an attempt to study the morphological and structural properties of the stable δ-phase Ho doped Bi_2O_3 nanocrystal powder ceramics. Also, the results of DC electrical conductivity measurements were showed as related to the conduction mechanism in the temperature range of 702–1169 K.

2. Experimental procedure

2.1. Materials and methods

In the experiment, bismuth(III) acetate (99.99%, Aldrich), holmium(III) acetate (99.99%, Aldrich) and polyvinyl alcohol (PVA) (Aldrich, molecular weight = 85,000–124,000) were used as starting materials and ultrapure deionized water was used as a solvent. PVA was obtained from Sigma Aldrich. Aqueous PVA solution (8%) was first prepared by dissolving PVA powder in distilled water and heating at 353 K with stirring for 3 h, then cooling to room temperature. Then, 1 g of bismuth(III) acetate and 0.2973 g of holmium(III) acetate were added to the 125 g aqueous PVA at 333 K separately and drop by drop and the solution was vigorously stirred for one hour at this temperature. Stirring was continued for 3 h at room temperature. Thus, viscous gels of PVA/Ho–Bi acetate hybrid polymer solution were obtained. Finally, the hybrid polymer solution was calcined at a rate of 8 K/min and remained for 2 h at 1100 K at atmospheric conditions.

The calcined materials were ground and pressed into a disk shape pellet using 13 mm die at 15 t/cm^2 uniaxially. To obtain long term phase stability, the pellets of the samples were subsequently sintered at 1023 K for 100 h in air for the conductivity measurements (Table 1).

2.2. Measurement and characterization

The pH and conductivity of the solutions were measured by using Wissenschaftlich–Technische–Werkstätten WTW and 315i/SET apparatus. The viscosity of the hybrid polymer solutions was measured with AND SV-10 viscometer. The surface tension of the complex hybrid polymer solution was measured by using KRUSS model manual measuring system. Composite morphology was taken by scanning electron microscopy JEOL JSM 6060 on samples sputtered with gold and observed at an accelerating voltage of 10 kV. Particles diameter was measured by image processing software, ImageJ (Image Pro-Express, Version 5.0.1.26, Media Cybernetics Inc.). ImageJ is a public domain Java image processing program. The crystal structures of the calcined powders were investigated by means of x-ray diffraction XRD Bruker AXS D8 Advance, Cu Kα radiation, 1.54–1.56 Å.

Thermal behavior of the samples was determined by using a Thermo Gravimetry/Differential Thermal Analyzer (TG/DTA) system. The TG/DTA measurements were performed in an alumina crucible, using a Perkin Elmer-Diamond analyzer (heating-cooling rate 10 K/min). The detected phase transformations were compared with the results of XRD patterns. The final phase of the samples was also identified by XRD and DTA measurements after each conductivity measurement experiments.

The electrical conductivity of the disk shape pellet samples was determined by using DC four-point probe technique in air. Standard DC four-point probe conductivity measurements were carried out by using Pt wire electrodes which is connected to a Keithley 2400 sourcemeter and 2700 multimeter. The measured data were transferred to a PC through interface card and by using a visual basic code program.

3. Results and discussion

3.1. Structural analysis

Fig. 1 shows the XRD patterns of the calcined Ho_2O_3 doped Bi_2O_3 nanoceramic powders at room temperature. XRD patterns revealed that holmia stabilized δ-phase Bi_2O_3 composite ceramic powder samples calcined at 1123 K are composed of a solid solution series with fluorite type face-centered cubic (fcc) symmetry δ-phase. The fcc δ-phase structure clearly appeared and, according to JCPDS-International Center for Diffraction Data, (01-088-1053) corresponds to a typical XRD spectrum of holmia stabilized δ-phase Bi_2O_3 for calcined powder. The reflection peaks appeared at $2\theta = 27.97^\circ$ (111), 32.63° (200), 46.43° (220), 55.29° (311), 57.79° (222), 74.32° (420), and 86.63° (422) and are in good agreement with the observed and calculated values.

The SEM micrograph of the sample is shown in Fig. 2a and b. The micrograph of the sample contains almost fluently

Table 1

Solution	*pH*	*Viscosity* (mPa s)	*Conductivity* (mS cm^{-1})	*Surface tension* (mN m^{-1})
Ho doped Bi_2O_3	3.29	418.2	1.369	54

distributed and spherical shaped grains. The presence of voids of irregular dimensions indicates that the powders have certain degree of porosity.

The grain size diameter distribution graph is given in Fig. 3. According to grain size diameter distribution, average grain size is calculated about 47.4 nm.

Fig. 4 shows the Fourier transform infrared spectrum of the holmium doped Bi_2O_3 nanoceramic powders. The vibrational bands observed at 2889 and 2980 cm^{-1} refer to the stretching C–H vibration of alkyl groups. This means that no water vapor can absorb on the surface of the ceramic powder and all the carbons were removed after being calcined. Bi–O bonds stretching vibrations in strongly distorted BiO_6 polyhedra (466 cm^{-1}), Bi–O bonds vibrations in strongly distorted BiO_6 units (556 cm^{-1}), the vibration absorption bands of the Bi–O–Bi (846 cm^{-1}), and Bi(3)–O–Bi(6) specific vibrations (921 cm^{-1}) were clearly observed in the FT-IR spectrum for the holmium doped Bi_2O_3 nanoceramic powders [18,19].

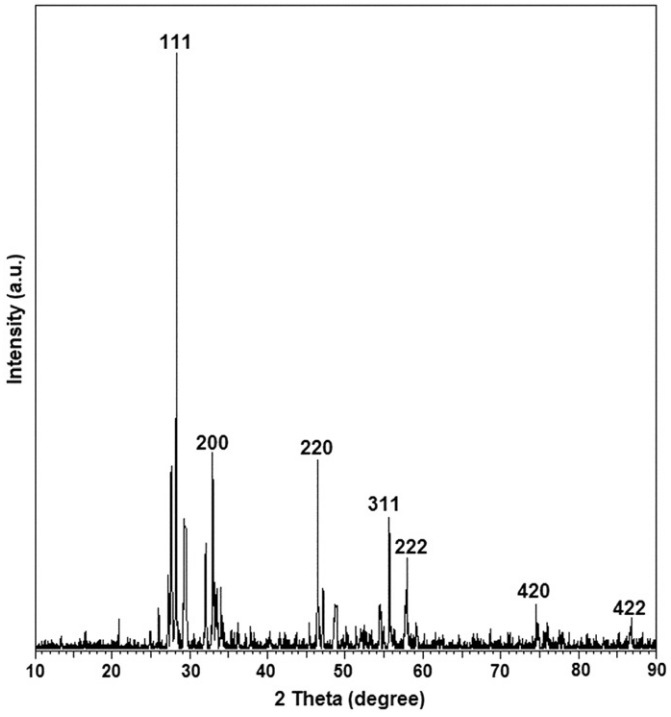

Fig. 1. The XRD patterns of the Ho-doped Bi_2O_3 nanoceramic powder.

3.2. Thermal analysis

Thermal behavior of the samples, which is observed using the TG/DTA system, is given in Fig. 5. The TG results (red line) show the weight loss of the sample during the thermal treatment of the measurement time. The TG curve indicates that there is almost no mass loss during heating and cooling process, which means that the sample will be stay stable at even high temperature operations. The DTA results (blue line) show a broad endothermic peak in between 930 and 960 K during heating process. This peak disappeared when the sample cooled down. The DTA curve, which is an indication of thermal behavior of the sample, demonstrates that the broad endothermic peak can be due to the order–disorder transition (ODT) rather than the phase transition.

There are two distinct regions of the conductivity curve in Fig. 6 which also indicate a transition occurring at 973 K. In addition, the electrical conductivity measurements show that there is a sharp increase in electrical conductivity at around 973 K which can be the evidence of the ODT. The ODT is a higher-order or critical point transition [20]. The order parameter of the transition is the occupation of sublattice of the fcc δ-phase Bi_2O_3 which has some oxygen ion vacancies in structure that is described as

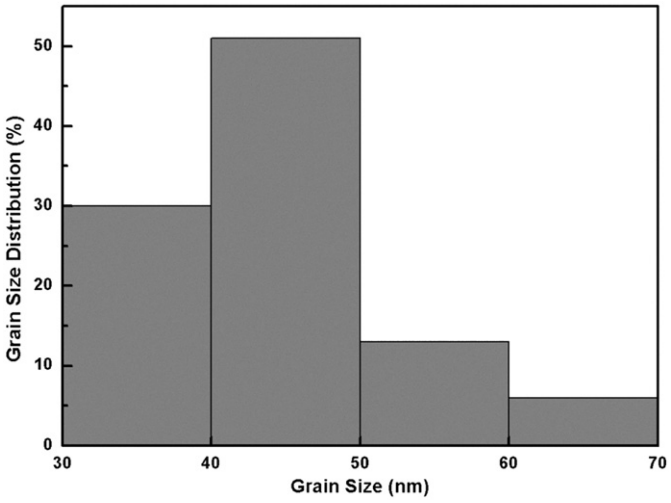

Fig. 3. Grain diameter distribution graph of holmium doped Bi_2O_3 nanoceramic powder.

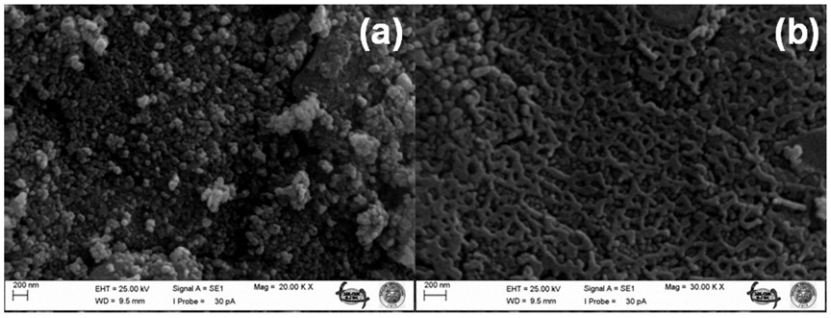

Fig. 2. SEM images of the Ho-doped Bi_2O_3 ceramic powders at (a) low magnification, and (b) high magnification.

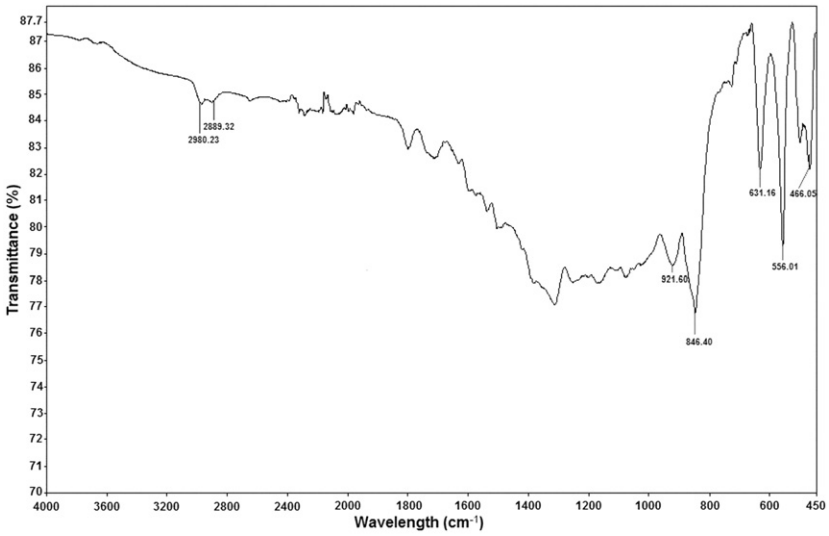

Fig. 4. FTIR spectrum of the holmium doped Bi_2O_3 nanoceramic powder.

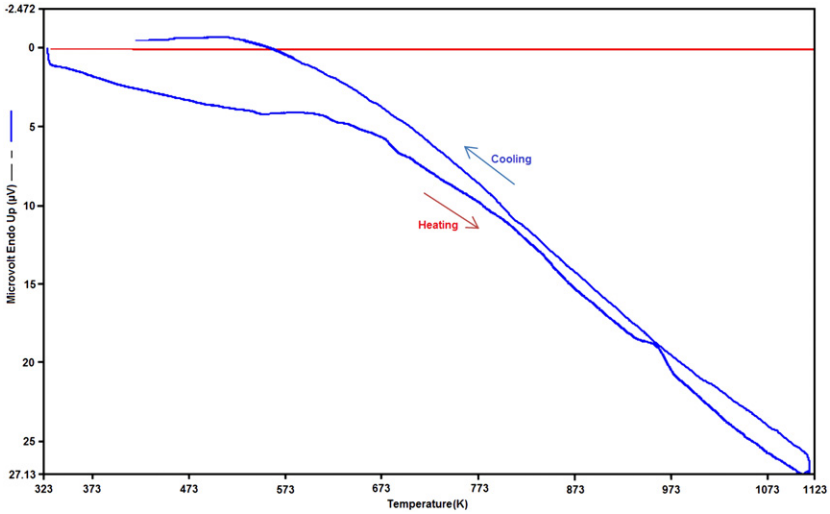

Fig. 5. Thermal behavior of the Ho-doped Bi_2O_3 ceramic powders obtained by using the TG/DTA system.

the distorted defect crystal structure. The oxygen lattice points of the Ho_2O_3 doped δ-phase Bi_2O_3 are not completely occupied with oxygen ions. Through the solid state reactions of Bi_2O_3 doped with Ho_2O_3, Ho^{3+} cations preferentially substitute at the fcc sites in the crystal structure. This was an indication that Ho_2O_3 dissolves in δ-phase type Bi_2O_3 matrix. Some of the oxygen lattice points located around fcc sites may be vacant forming an oxygen vacancy. In the references, the fcc crystal structure has an oxygen deficient fluorite structure with two units, and two oxygen ion vacant sites per unit cell and bismuth ions in the structure are located on fcc sites, and differ only in the location of the oxygen ions [21].

It is clear that the transition between the low-temperature range (LTR) and high-temperature range (HTR) can be attributed to the ODT because the δ-phase is stable and preserved even at room temperature as shown by the XRD pattern of Fig. 1. So, the endothermic reaction and conductivity transition indicate the same transport mechanism which occurs due to oxide ion location site occupancy differences [22,23].

3.3. Electrical measurements

The DC electrical conductivity (σ_{DC}) of the Ho doped Bi_2O_3 nanoceramic powders was measured by the four-point probe method [24–26] in the temperature range from 702 to 1169 K. In this paper, low temperature measurements of conductivity were not taken into consideration because of poor conductivities for the studied sample. By using the four-point probe measurement technique, the measurement errors due to wire resistance, the spreading resistance under each wire, and the contact resistances between each metal wire and the samples were eliminated

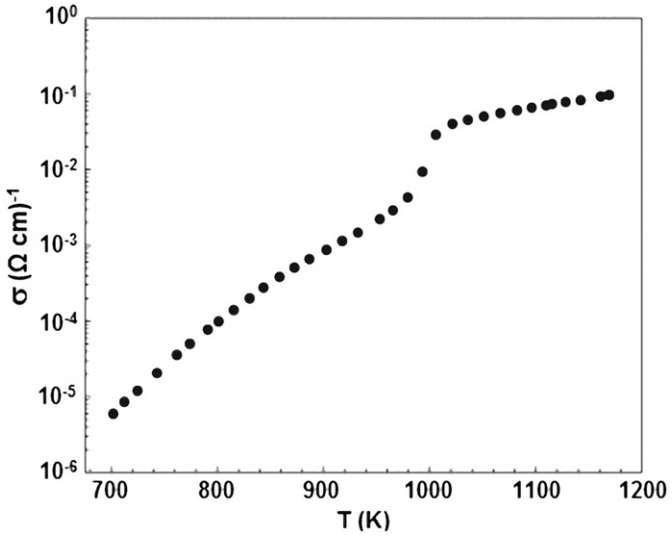

Fig. 6. Temperature dependence of σ_{DC} for Ho-doped Bi_2O_3 nanoceramic powder.

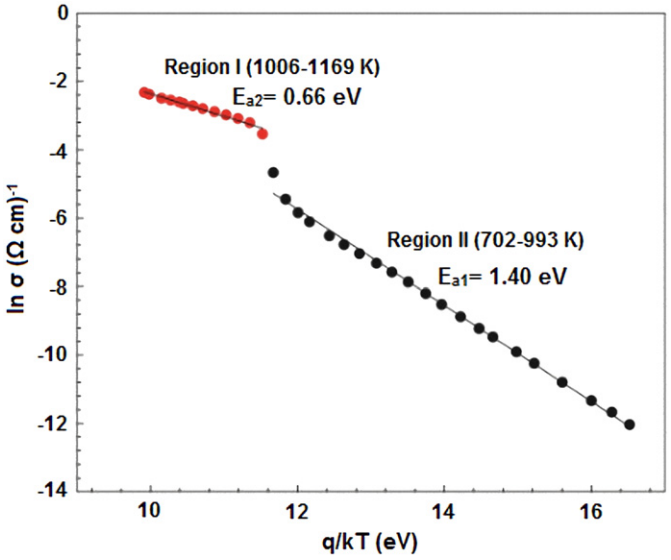

Fig. 7. The Arrhenius plot of σ_{DC} for Ho-doped Bi_2O_3 nanoceramic powder.

[25]. The electrical conductivity measurements were carried out in the temperature ranging from room temperature to just below melting point of circular-shaped pellet samples. The measuring unit was interfaced with a PC for on-line data acquisition and processing. A Keithley 2400 source-meter was used to provide constant current and the potential drop was detected by a Keithley 2700 multimeter with a 7700 multiplexer switch card. Pt wires with a diameter of 0.5 mm were employed as current and potential probes. Electrical resistivity and conductivity were determined from the detected current and voltage drop using a standard conversion method [26]. The temperature of the sample was changed by a controllable Nabertherm furnace. The temperature of the samples was also measured using a 0.5 mm standard *K* type thermocouple which was placed very close to the sample and detected with the Keithley 2700 multimeter.

The DC electrical conductivity (σ_{DC}) is a thermally activated process. Fig. 6 shows the temperature dependence of σ_{DC} for Ho-doped Bi_2O_3 nanoceramic powders. As a consequence of structural changes, electrical conductivity could be profoundly modified. The DC conductivity almost linearly increases with increasing temperature, which may result from charge transport through extended bands [27]. As can be seen in Fig. 6 σ_{DC} vs. T plot shows two linear regions with different slopes. Such behavior of this plot shows that the existence of two different conduction mechanisms is effective in the measured temperature range. The temperature dependence of σ_{DC} also indicates that the electrical conduction in the ceramic material is governed by the Arrhenius relation

$$\sigma = \sigma_0 \exp(-E_a/k_B T) \quad (1)$$

where σ is the pre-exponential factor, E_a is the activation energies of the mobile charge carriers, k_B is the Boltzmann's constant and T is the temperature in K.

The Arrhennius ($\ln(\sigma_{DC})$ vs. q/kT) plot of the studied sample was given in Fig. 7. It is clear that two linear regions with different slopes were discerned. The activation energies for two different temperature regions were calculated from the slopes of the straight lines of the $\ln \sigma_{DC}$ vs. q/kT plot. The activation energies E_{a1} and E_{a2}, which are corresponding to the temperature range of 702–993 K and 1006–1169 K, respectively, were found to be 1.40 and 0.66 eV. The difference between two activation energies of conducting process is due probably to the instability of the Bi_2O_3 nanoceramic powders in the mentioned temperature range. Oxygen vacancies and space charge polarization may be responsible for the change in activation energy as a function of temperature. Oxygen vacancies may be created with an increase in the temperature. This is expected because the conductive activation energy is measured at higher temperatures and related to the long-distance diffusion of oxygen ions, while the relaxation activation energy is measured at lower temperatures and related to the short-distance jumps of oxygen ions [28]. It is well known that oxides usually have an excess of oxygen vacancies at high temperatures, a further increase in the content of oxygen vacancies through the introduction of respective additives delays diffusion, obstructs the polymorphic transition, and stabilizes the phase [29]. Introduction of additives which increase the concentration of cation vacancies, on the contrary, accelerates diffusion and facilitates the polymorphic transition. In this case, at high temperatures, the activation energy (relaxation energy) is large enough to create vacancies which are a sum of energy required for vacancy creation and motion of charge carriers into vacancies [30,31].

4. Conclusions

In this study, a sol–gel combustion technique was used to synthesize Ho-doped Bi_2O_3 nanoceramic powders. The morphology, structure, and the DC conductivity of

Ho-doped Bi_2O_3 nanoceramic materials have been investigated. The XRD results show that the nanoceramic samples have the stable high conductive fcc δ-phase preserved down to the room temperature. This result is supported by DTA and electrical conductivity results which also show the order–disorder transition at the temperature around 973 K. Conductivity versus temperature response is linear in the wide temperature range and it gives small deviation at 1006 K. This can be explained by thermally activated process. Arrhenius plot of Ho-doped Bi_2O_3 nanoceramic materials gives two different straight lines with different slopes. Two temperature ranges characterized by different activation energies indicate that the space charge and oxygen ion vacancies are important in the conduction process.

Acknowledgments

One of us (M. Ari) would like to thank the Erciyes University's Research Fund for financially supported (Project no.: FBA-11–3525).

References

[1] C.Y. Yoo, B.A. Boukamp, H.J.M. Bouwmeester, Oxygen surface exchange kinetics of erbia-stabilized bismuth oxide, Journal of Solid State Electrochemistry 15 (2011) 231–236.

[2] G.H. Zhong, J.L. Wang, Z. Zeng, The doping effects in δ-Bi_2O_3 oxide ionic conductor, Physica Status Solidi B 12 (2008) 2737–2742.

[3] A.A. Yaremchenko, V.V. Kharton, E.N. Naumovich, A.A. Vecher, Oxygen ionic transport in Bi_2O_3-based oxides: the solid solutions Bi_2O_3–Nb_2O_5, Journal of Solid State Electrochemistry 2 (1998) 146–149.

[4] Ş. Durmuşoğlu, S. Keskin, I. Uslu, A. Aytimur, A. Akdemir, Synthesis and characterization of Bi_2O_3-doped with lanthanum by electrospinning method, International Journal of Material Science and Electronics Research 1 (2010) 81–85.

[5] Ş. Durmuşoğlu, I. Uslu, T. Tunç, S. Keskin, A. Aytimur, A. Akdemir, Synthesis and characterization of boron-doped Bi_2O_3–La_2O_3 fiber derived nanocomposite precursor, Journal of Polymer Research 18 (2011) 1999–2004.

[6] T. Tunç, I. Uslu, Ş. Durmuşoğlu, S. Keskin, A. Aytimur, A. Akdemir, Preparation of gadolina stabilized bismuth oxide doped with boron via electrospinning technique. Journal of Inorganic and Organometallic Polymers, http://dx.doi.org/10.1007/s10904-011-9531-5.

[7] M. Drache, P. Roussel, J.P. Wignacourt, Structures and oxide mobility in Bi–Ln–O materials: heritage of Bi_2O_3, Chemical Reviews 107 (2007) 80–86.

[8] S. Arasteh, A. Maghsoudipour, M. Alizadeh, A. Nemati, Effect of Y_2O_3 and Er_2O_3 co-dopants on phase stabilization of bismuth oxide, Ceramics International 37 (2011) 3451–3455.

[9] F. Krok, I. Abrahams, H. Holdynski, A. Kozanecka-Szmigiel, M. Malys, M. Struzik, X. Liu, J.R. Dygas, Oxide ion distribution and conductivity in $Bi_7Nb_{2-2x}Y_{2x}O_{15.5-2x}$, Solid State Ionics 179 (2008) 975–980.

[10] M. Yashima, D. Ishimura, Visualization of the diffusion path in the fast oxide-ion conductor $Bi_{1.4}Yb_{0.6}O_3$, Applied Physics Letters 87 (2005) 221909.

[11] M. Ari, B. Saatçi, M. Gündüz, F. Meydaneri, M. Bozoklu, Microstructure and thermo-electrical transport properties of Cd–Sn alloys, Materials Characterization 59 (2008) 624–630.

[12] M.G. Lazarraga, F. Pico, J.M. Amarilla, R.M. Rojas, J.M. Rojo, The cubic $Bi_{1.76}U_{0.12}La_{0.12}O_{3.18}$ mixed oxide: synthesis, structural characterization, thermal stability and electrical properties, Solid State Ionics 176 (2005) 2313–2318.

[13] S.S. Cetin, I. Uslu, A. Aytimur, S. Ozcelik, Characterization of Mg doped ZnO nanocrystallites prepared via electrospinning. Ceramics International, http://dx.doi.org/10.1016/j.ceramint.2012.02.003.

[14] A. Aytimur, I. Uslu, S. Koçyiğit, F. Özcan, Magnesia stabilized zirconia doped with boron, ceria and gadolinia. Ceramics International, http://dx.doi.org/10.1016/j.ceramint.2012.01.035.

[15] R. Riedel, G. Mera, R. Hauser, A. Klonczynski, Silicon-based polymer-derived ceramics: synthesis properties and applications—a review, Journal of the Ceramic Society of Japan 114 (6) (2006) 425–444.

[16] M.A. Schiavon, K.J. Ciuffi, I.V.P. Yoshida, Glasses in the Si–O–C–N system produced by pyrolysis of polycyclic silazane/siloxane networks, Journal of Non-Crystalline Solids 353 (2007) 2280–2288.

[17] M.A. Schiavon, I.V.P. Yoshida, Ceramic matrix composites derived from $CrSi_2$-filled silicone polycyclic network, Journal of Materials Science 39 (2004) 4507–4514.

[18] M. Bosca, L. Pop, G. Borodi, P. Pascuta, E. Culea, XRD and FTIR structural investigations of erbium-doped bismuth–lead–silver glasses and glass ceramics, Journal of Alloys and Compounds 479 (2009) 579–582.

[19] D. Rusu, I. Ardelean, Structural studies of Fe_2O_3–Bi_2O_3–CdO glass system, Materials Research Bulletin 43 (2008) 1724–1730.

[20] J.R. Waldram, The Theory of Thermodynamics, Cambridge University Press, Cambridge, 1985.

[21] K.R. Kendall, C. Navas, J.K. Thomas, H.C. zur Loye, Recent developments in oxide ion conductors: aurivillius phases, Chemistry of Materials 8 (1996) 642–649.

[22] J. Jeong, E.J. Lee, Y.H. Han, Effects of Ho_2O_3 addition on defects of $BaTiO_3$, Materials Chemistry and Physics 100 (2006) 434–437.

[23] K.J. Park, C.H. Kim, Y.J. Yoon, S.M. Song, Y.T. Kim, K.H. Hur, Doping behaviors of dysprosium, yttrium and holmium in $BaTiO_3$ ceramics, Journal of the European Ceramic Society 29 (2009) 1735–1741.

[24] Y. Liu, A.R. West, Ho-doped BaTiO3: polymorphism, phase equilibria and dielectric properties of $BaTi_{1-x}Ho_xO_{3-x}/2$: $0 \le x \le 0.17$, Journal of the European Ceramic Society 29 (2009) 3249–3257.

[25] F.M. Smits, Measurement of sheet resistivities with the four point probe, The Bell System Technical Journal 37 (1958) 711–718.

[26] B. Saatci, M. Ari, M. Gündüz, F. Meydaneri, M. Bozoklu, S. Durmus, Thermal and electrical conductivity of Cd–Zn alloys, Journal of Physics: Condensed Matter 18 (2006) 10643–10653.

[27] A.S. Riad, M.T. Korayem, T.G. Abdel-Malik, AC conductivity and dielectric measurements of metal-free phthalocyanine thin films dispersed in polycarbonate, Physica B 270 (1999) 140–147.

[28] D. Li, X.P. Wang, Q.F. Fang, J.X. Wang, C. Li, Z. Zhuang, Phase transition associated with the variation of oxygen vacancy/ion distribution in the oxide-ion conductor $La_2Mo_{2-x} \cdot W_xO_9$, Physica Status Solidi A 7 (2007) 2270–2278.

[29] A.V. Belyakov, Stabilization of polymorphic phases in oxides. Polymorphic transitions, Glass Ceramics 56 (1999) 52–54.

[30] S.K. Barik, R.N.P Choudhary, P.K. Mahapatra, Structural and electrical properties of $Na_{1/2}Gd_{1/2}TiO_3$ nanoceramics, Journal of Alloys and Compounds 459 (2008) 35–40.

[31] S.K. Patri, R.N.P Choudhary, B.K. Samantary, Dielectric and electrical properties of $Bi_9Fe_5Ti_4O_{29}$ nanoceramics, Journal of Alloys and Compounds 459 (2008) 333–337.